IOP PUBLISHING JOURNAL OF PHYSICS D: APPLIED PHYSICS

J. Phys. D: Appl. Phys. **42** (2009) 145113 (9pp) doi:10.1088/0022-3727/42/14/145113

Coupled electromechanical effects in II–VI group finite length semiconductor nanowires

Sunil R Patil and Roderick V N Melnik

M^{2}NeT Laboratory, Wilfrid Laurier University, 75 University Ave W, Waterloo, ON, N2L 3C5, Canada

E-mail: spatil@wlu.ca and rmelnik@wlu.ca

Received 8 January 2009
Published 1 July 2009
Online at stacks.iop.org/JPhysD/42/145113

Abstract

In this contribution the electromechanical effects in II–VI group semiconductor finite length embedded nanowires (NWs) are analysed with fully coupled models of electroelasticity. First, strain distributions are obtained using analytical expressions derived from the Eshelby formulation with an assumption of isotropy. These results are then compared with general three-dimensional model based calculations, accounting for anisotropy and piezoelectricity. Next, as representatives of group II–VI NW systems we take zincblende CdTe/ZnTe and wurtzite CdSe/CdS crystal structured materials. The detailed analysis of strain relaxation along with electromechanical distributions are presented for common cross-sectional shapes of NWs such as triangular, square and crescent. Comparative results for both models, analytic and numerical, are presented and their applicability is discussed. The effects of the finite length of the NWs on electromechanical distributions are also discussed.

(Some figures in this article are in colour only in the electronic version)

1. Introduction

Wide band-gap semiconductor nanostructures have attracted much attention due to their current and potential applications in electronics and optoelectronics. III–V semiconductor nanostructures, in particular GaN- and GaAs-based nanostructures, are the leading materials in many nanotechnological areas [1–3]. However, there are certain limitations, such as large internal piezoelectric field and spontaneous polarization observed in these materials, requiring higher carrier densities to generate optical gain [4]. To overcome such difficulties, II–VI semiconductor nanostructures provide a viable alternative, in particular CdTe- and ZnSe-based nanostructures [5]. Apart from this, II–VI semiconductor nanostructures are prospective candidates for many electronic and optoelectronic applications including light emitters [6–8], elements of solar cells [9], transparent conductive layers or buffer thin films [10] and CdTe, CdSe and CdS nanowires (NWs) based infra-red detection [11, 12].

Advances in growth technologies now make it possible to grow high quality nanostructures [13–15]. As these nanostructures are often formed through heteroepitaxy, they exhibit lattice mismatched strain [16, 17], strain-induced piezoelectric, spontaneous polarization [18], coupled thermopiezoelectromechanical [19] and nonlinear electromechanical effects [20]. Apart from this, nanoscale size effects also lead to piezoelectricity in non-piezoelectric materials [21]. Several studies [8, 16, 22, 23] show that the electromechanical effects play a key role in engineering electronic and optoelectronic properties of NW and other low dimensional semiconductor nanostructures. In particular, these effects are important in the transitions of type-I to type-II semiconductor heterostructures [7], rigid shifts in band edges and modifications of valance band structures [16, 22], as well as in unsymmetric wavefunctions in crescent NWs [23]. Most of these studies are focused mainly on III–V group semiconductor nanostructures [2, 4, 22, 24, 25], whereas relatively less work has been done in this context on II–VI group semiconductor nanostructures [8]. Also, experimental observations of dimensional effects on the electronic structure of CdTe NWs have recently been reported [26]. All this indicates that a systematic study providing details of strain relaxation, strain-induced piezoelectric and spontaneous polarization effects in finite II–VI nanostructures is becoming increasingly important.

As a first approximation from the field of continuum mechanics, the well-known Eshelby inclusion method has been applied to study the induced strain/electric fields in low dimensional nanostructures and in particular to NW [16, 17, 22, 25, 27–29]. The advantage of the Eshelby inclusion method is its simplicity as the induced electromechanical fields can be found analytically. However, the resulting analytical representation leads to well-known difficulties pronounced in the appearance of singularities, in particular, for line segments, at the vertices and for circular arcs, at the centre of the corresponding circle [17]. Apart from this, although the lattice misfit between NW and matrix can be accounted for, the Eshelby inclusion method assumes isotropy of the NW system [16, 17, 22, 25, 27–29]. Under these conditions, the semi-coupled formulation based on strain calculated from the Eshelby inclusion method and the Poisson equation for electrostatics allows us to calculate strain-induced electric fields. However, the semi-coupled formulation for piezoelectricity was found to be inaccurate as compared with the fully coupled formulation [18] and it is known that the assumption of isotropy may lead to more than 10% error in strain calculations [30]. Therefore, in order to enhance electronic/optoelectronic performance, a systematic study of electromechanical effects in II–VI NWs with fully coupled models is required. This is particularly true for practical situations involving finite length NWs.

Noting that bandstructure calculations of NWs have been carried out in a series of publications [31–35], in this paper we focus on the electromechanical effects in the II–VI group embedded finite length NWs. II–VI semiconductor materials are generally crystallized in either the cubic zincblende (ZB) phase or the wurtzite (WZ) phase, but, for each material, one or the other of these phases is thermodynamically more stable at room temperature. Hence, we consider CdTe/ZnTe (ZB) and CdSe/CdS (WZ) NW systems, as representative examples of II–VI group semiconductors. We focus on electromechanical fields in NWs of basic cross-sectional shapes such as triangular, square and crescent, like [14, 15], and we refer to them from hereon as triangular, square and crescent-shaped NWs. First, we obtain strain distributions using the Eshelby inclusion method and then compare them with our results obtained with a more general three-dimensional (3D) model accounting for anisotropy and piezoelectricity. We provide details on electromechanical effect contributions in WZ and ZB NWs and analyse the importance of the application of a general 3D model. The effects of the finite length of the NWs on electromechanical distributions are also discussed.

2. Theoretical formulations

In what follows, we briefly highlight the main features of inclusion theory, followed by a detailed description of a fully coupled 3D multi-physics model and corresponding constitutive relations for ZB and WZ crystals.

2.1. Inclusion method

First, we assume that the NWs are buried in an infinite medium so that the effect of free surfaces is neglected [28]. The NW and host matrix materials are assumed to be continuous, linear, isotropic and to obey Hooke's laws. In this simplified case the stress components at position (x, y) are determined by evaluating the contour integral [27, 36]:

$$\sigma_{ij}(x, y) = \oint \boldsymbol{A}_{ij}(x_0 - x, y_0 - y) \cdot \mathrm{d}\boldsymbol{r}, \tag{1}$$

where the contour integration is performed around the boundary of the NW in the counter-clockwise sense and (x_0, y_0) are points on the boundary. The vectors $\boldsymbol{A}_{ij}$ are chosen so that $\nabla \times \boldsymbol{A}$ yields the cylindrical Green's function components [27]. In this case, the analytical expressions for straight lines and circular arcs can be derived (see [28] for detailed expressions). The strain components can be obtained using Hooke's laws.

2.2. 3D electromechanical model

We formulate a mathematical model, based on coupled multi-physics governing equations in order to study the electromechanical effects in NWs. Although in some special cases the model can be reduced to a 2D representation, piezoelectric coupling, which appears through shear components in ZB crystals [18], is required to solve this problem using the full 3D model. The problem is governed by a coupled system of equilibrium equations of elasticity and electrostatics. The 3D linear fundamental equations for the electromechanical structure occupying volume Ω, under steady state conditions, can be summarized as follows:
mechanical equilibrium equation,

$$\nabla \cdot \sigma + f = 0, \tag{2}$$

the equation of electrostatics,

$$\nabla \cdot D - q = 0, \tag{3}$$

where σ is the stress tensor, D is the electric displacement vector, f and q are body mechanical force and electric charge in Ω, respectively. The following are the gradient equations that correspond to the relationships between the linear strain-mechanical displacements and the electric field-electric potential. They are stated, respectively, as

$$\varepsilon_{kl} = \frac{1}{2}\left(\frac{\partial u_k}{\partial x_l} + \frac{\partial u_l}{\partial x_k}\right), \qquad E_k = -\frac{\partial V}{\partial x_k}, \tag{4}$$

where ε_{kl}, E_k, u and V are the components of the strain tensor, electric field vector, mechanical displacement vector and electric potential, respectively. Coupling between equations (2) and (3) is implemented through constitutive equations described as follows:
for ZB crystals,

$$\begin{aligned}
&\sigma_{xx} = C_{11}\varepsilon_{xx} + C_{12}\varepsilon_{yy} + C_{12}\varepsilon_{zz},\\
&\sigma_{yy} = C_{12}\varepsilon_{xx} + C_{11}\varepsilon_{yy} + C_{12}\varepsilon_{zz},\\
&\sigma_{zz} = C_{12}\varepsilon_{xx} + C_{12}\varepsilon_{yy} + C_{11}\varepsilon_{zz},\\
&\sigma_{xy} = 4C_{44}\varepsilon_{xy} - e_{14}E_z, \qquad \sigma_{yz} = 4C_{44}\varepsilon_{yz} - e_{14}E_x,\\
&\sigma_{zx} = 4C_{44}\varepsilon_{zx} - e_{14}E_y,\\
&D_x = e_{14}\varepsilon_{yz} + \in_{11} E_x, \qquad D_y = e_{14}\varepsilon_{zx} + \in_{11} E_y,\\
&D_z = e_{14}\varepsilon_{xy} + \in_{33} E_z,
\end{aligned} \tag{5}$$

Table 1. Physical parameters of ZB CdTe, ZnTe, CdSe and CdS.

Constants	CdTe	ZnTe	CdSe	CdS
Stiffness coefficient (GPa)				
c_{11}	53.3 [8]	71.3 [8]	74.6 [37]	90.68 [38]
c_{12}	36.5 [8]	40.7 [8]	46.1 [37]	58.09 [38]
c_{13}	—	—	39.3	50.9 [38]
c_{33}	—	—	81.7 [37]	93.8 [38]
c_{44}	20.1 [39]	31.0 [39]	13.0 [37]	14.3 [40]
Permittivity				
Υ_{11}	10.6 [41]	9.67 [42]	9.29 [37]	8.28 [44]
Υ_{33}	—	—	10.16 [37]	8.73 [44]
Piezoelectric coefficient ($\mathrm{C\,m^{-2}}$)				
e_{14}	0.035 [43]	0.047 [45]	—	—
e_{15}	—	—	−0.138 [37]	−0.212 [45]
e_{31}	—	—	−0.16 [37]	−0.265 [45]
e_{33}	—	—	0.347 [37]	0.385 [45]
Young's modulus E (GPa)	42.4 [47]	51.2 [48]	43.1 [45]	48.1 [45]
Poisson ratio ν	0.408 [47]	0.363 [47]	0.37 [45]	0.37 [45]
Spontaneous polarization P^{sp} ($\mathrm{C\,m^{-2}}$)	0.0	0.0	0.006 [49]	0.002 [49]
Lattice constant (Å)				
a	6.482 [8]	6.1 [8]	4.3 [45]	4.135 [45]
c	6.482	6.1	7.01 [45, 46]	6.749 [45, 46]

and for WZ crystals,

$$\sigma_{xx} = C_{11}\varepsilon_{xx} + C_{12}\varepsilon_{yy} + C_{13}\varepsilon_{zz} - e_{31}E_z,$$

$$\sigma_{yy} = C_{12}\varepsilon_{xx} + C_{11}\varepsilon_{yy} + C_{13}\varepsilon_{zz} - e_{31}E_z,$$

$$\sigma_{zz} = C_{13}\varepsilon_{xx} + C_{13}\varepsilon_{yy} + C_{33}\varepsilon_{zz} - e_{33}E_z,$$

$$\sigma_{xy} = \frac{C_{11} - C_{12}}{2}\varepsilon_{xy},$$

$$\sigma_{yz} = C_{44}\varepsilon_{yz} - e_{15}E_y, \quad \sigma_{zx} = C_{44}\varepsilon_{zx} - e_{15}E_x,$$

$$D_x = e_{15}\varepsilon_{xz} + \in_{11} E_x, \quad D_y = e_{15}\varepsilon_{yz} + \in_{11} E_y,$$

$$D_z = e_{31}\varepsilon_{xx} + e_{31}\varepsilon_{yy} + e_{33}\varepsilon_{zz} + \in_{33} E_z + P^{sp}. \tag{6}$$

To take into account the lattice mismatch, the strain tensor components in equation (4) take the following form:

$$\varepsilon_{xx} = \frac{\partial u_x}{\partial x} - \varepsilon_a^*, \qquad \varepsilon_{yy} = \frac{\partial u_y}{\partial y} - \varepsilon_a^*,$$

$$\varepsilon_{zz} = \frac{\partial u_z}{\partial z} - \varepsilon_c^*, \qquad \varepsilon_{xy} = \frac{1}{2}\left(\frac{\partial u_x}{\partial y} + \frac{\partial u_y}{\partial x}\right),$$

$$\varepsilon_{yz} = \frac{1}{2}\left(\frac{\partial u_y}{\partial z} + \frac{\partial u_z}{\partial y}\right), \qquad \varepsilon_{zx} = \frac{1}{2}\left(\frac{\partial u_z}{\partial x} + \frac{\partial u_x}{\partial z}\right), \tag{7}$$

with $\varepsilon_a^* = (a_\mathrm{m} - a_\mathrm{w})/a_\mathrm{w}$ and $\varepsilon_c^* = (c_m - c_w)/c_w$ inside the NW and zero otherwise. Quantities a_m, c_m and a_w, c_w are the lattice constants of the matrix and the wire, respectively, while quantities ε_a^* and ε_c^* are the local intrinsic strains (lattice mismatch) along the a and c directions, respectively. The directions a and c correspond to the shorter and longer dimensions of the unit cell of the wurtzite crystal, respectively. In the case of ZB crystal, $a = c$.

The hydrostatic strain component is given by

$$\varepsilon_\mathrm{vol} = \varepsilon_{xx} + \varepsilon_{yy} + \varepsilon_{zz}. \tag{8}$$

The hydrostatic strain component is particularly important due to the fact that it provides information about rigid shift in energy subbands [17, 22]. In the plane stress case, by applying a 2D analytical method, it can be defined as $\varepsilon_\mathrm{vol} = 2\varepsilon_a^*(1 - 2\nu)/(1 - \nu))$ [27].

The per cent misfit strain in the case of the CdTe/ZnTe system is $\varepsilon_a^* = \varepsilon_c^* = (a_\mathrm{m} - a_\mathrm{w})/a_\mathrm{w} \times 100\% = -5.89\%$ and for CdSe/CdS, it is $\varepsilon_a^* = (a_\mathrm{m} - a_\mathrm{w})/a_\mathrm{w} \times 100\% = -3.99$ % and $\varepsilon_c^* = (c_m - c_w)/c_w \times 100\% = -3.87\%$, along a and c directions, respectively. We assume that the WZ NWs are oriented such that the c-direction of the crystal is along the z-axis. The electromechanical parameters used in the calculations are given in table 1.

3. Results and discussion

First, we obtain strain fields for triangular, square and crescent CdTe/ZnTe and CdSe/CdS NWs using a conventional 2D analytical method. Next, electromechanical distributions are obtained using our general 3D model for the same NWs with the same material systems and shapes by accounting for anisotropy and piezoelectricity. We assume that the CdTe and CdSe NWs are embedded in ZnTe and CdS matrices, respectively. The dimensions in the x and y directions of the respective shaped NWs are kept the same for both methods of calculations, the 2D analytical and the general 3D model. The cross-sectional dimensions for NWs of different shapes are as follows: (a) for the triangular NWs, base of 10 nm and height of 10 nm, (b) for the square NWs, sides of 10 nm and (c) crescent NWs are 4 nm thick (in the y-direction) at the centre while ∼1 nm thick at the ends (in the x-direction), two ends are 8 nm apart (in the x-direction). The lengths for 3D calculations for all NWs are taken to be 40 nm (in the z-direction). In order to study length effects, we vary the length of the square NWs

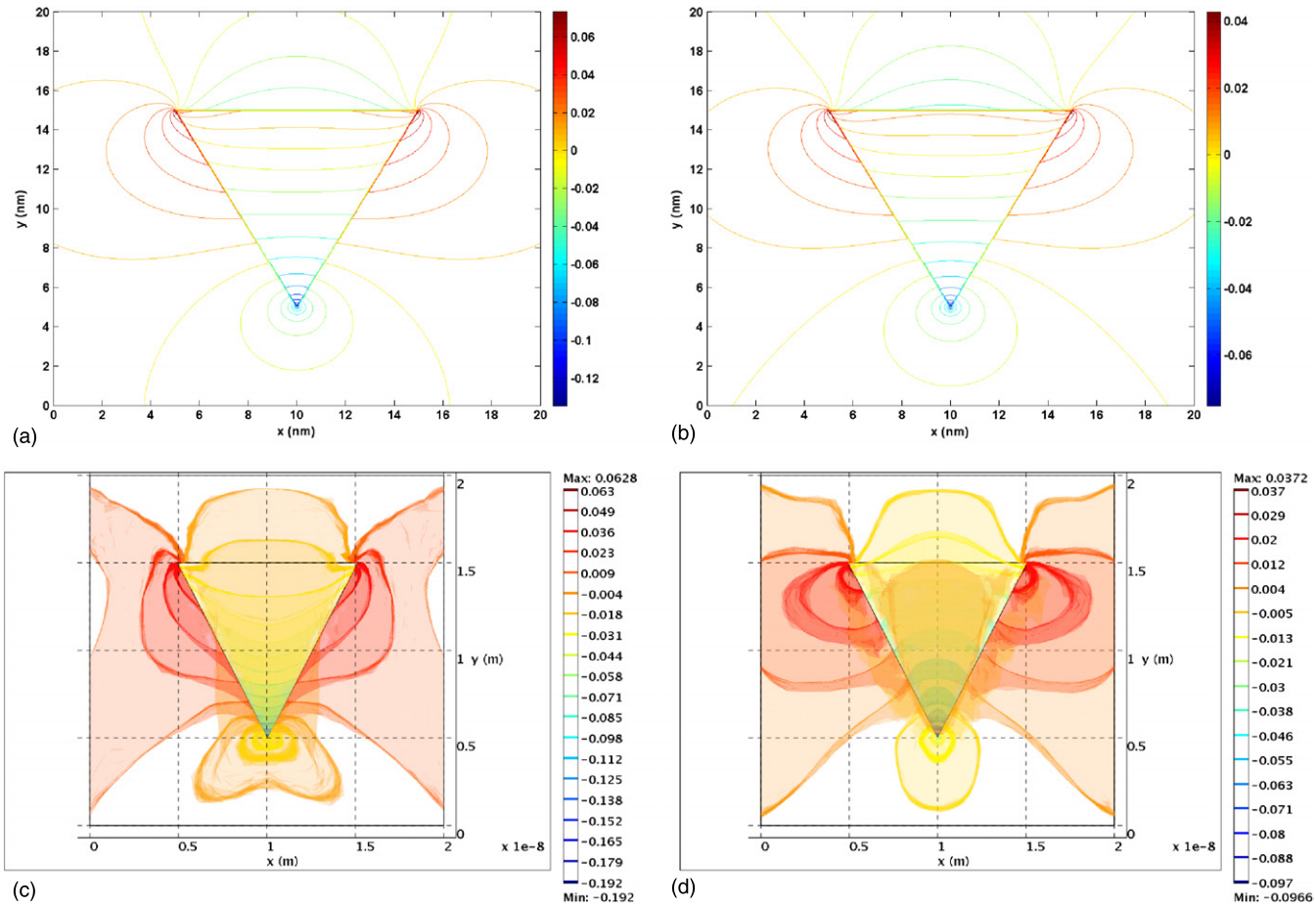

Figure 1. Strain distributions for the triangular NWs. (*a*) Inclusion based model, ε_{xx} for CdTe/ZnTe NW. (*b*) Inclusion based model, ε_{xx} for CdSe/Cds NW. (*c*) Our 3D model, ε_{xx} for Cdte/ZnTe NW. (*d*) Our 3D model, ε_{xx} for CdSe/Cds NW. (Colour online.)

from 40 to 10 nm. The matrix is assumed to have dimensions 20 nm × 20 nm × 60 nm for all NW systems.

Figure 1 shows the strain distributions for the triangular NWs made of CdTe/ZnTe (figures 1(*a*) and (*c*)) and CdSe/CdS (figures 1(*b*) and (*d*)). Figures 1(*a*) and (*b*) show the results obtained with the 2D analytical and figure 1(*c*) and (*d*) show the results obtained with the general 3D model. The strain magnitudes inside the NWs are similar, irrespective of the calculation methodology chosen. In all the cases the magnitude of the strain tensor components ε_{xx} is typically less than $\varepsilon_a^*/2$ (2.945 % for CdTe/ZnTe and 1.995% for CdSe/CdS) at all points inside the NWs except for the region near the apex of the triangle where the strains have higher magnitudes than $\epsilon_a^*/2$ and become highly irregular (figures 1(*a*) and (*b*)). Analytical results show that qualitatively strain distributions are similar for both NWs. These observations agree well with the previous results reported in the literature [17, 27]. In contrast to this, in the CdTe/ZnTe NWs, strain distributions obtained by the 2D analytical methodology are different from the results obtained with the general 3D model (compare figures 1(*a*) and (*c*)). However, they are very similar in the case of CdSe/CdS NWs. Both methodologies lead to qualitatively similar strain distributions in WZ NWs and slightly different distributions in the case of ZB NWs. We observe similar behaviour for other shapes of the NWs.

Figure 2 shows the electric potential for the square (figures 2(*a*) and (*b*)) and electric potential for the crescent shaped (figures 2(*c*) and (*d*)) NWs made of CdTe/ZnTe and CdSe/CdS, respectively. As a result of the WZ crystal structure of the CdSe/CdS NW system, orders of magnitude higher electric potentials are observed as compared with the CdTe/ZnTe NWs. However, the actual values are still much smaller compared with typical GaN-based nanostructures [4]. There is a notable qualitative difference in the electric field and potential distributions in these two materials. In the case of ZB CdTe/ZnTe, higher values of electric field and potential are observed at corners whereas in WZ CdSe/CdS they are observed at the interface centres of the NWs. This can be explained by the fact that CdSe/CdS has hexagonal symmetry which is a better approximation to the cylindrical symmetry compared with the cubic symmetry of CdTe/ZnTe. Similar features to those observed in triangular and square NWs are also observed in crescent NWs for their respective materials. In general, strain fields inside the NWs are much higher compared with the values of strain in the substrates [25]. The qualitative features, such as different strain distributions in WZ and ZB materials and a preferred region of electric potential observed with the general 3D model, cannot be explained with the conventional 2D analytical model.

Figure 3 shows the principal strain components (figure 3(*a*)), the hydrostatic strain component, ε_{vol}

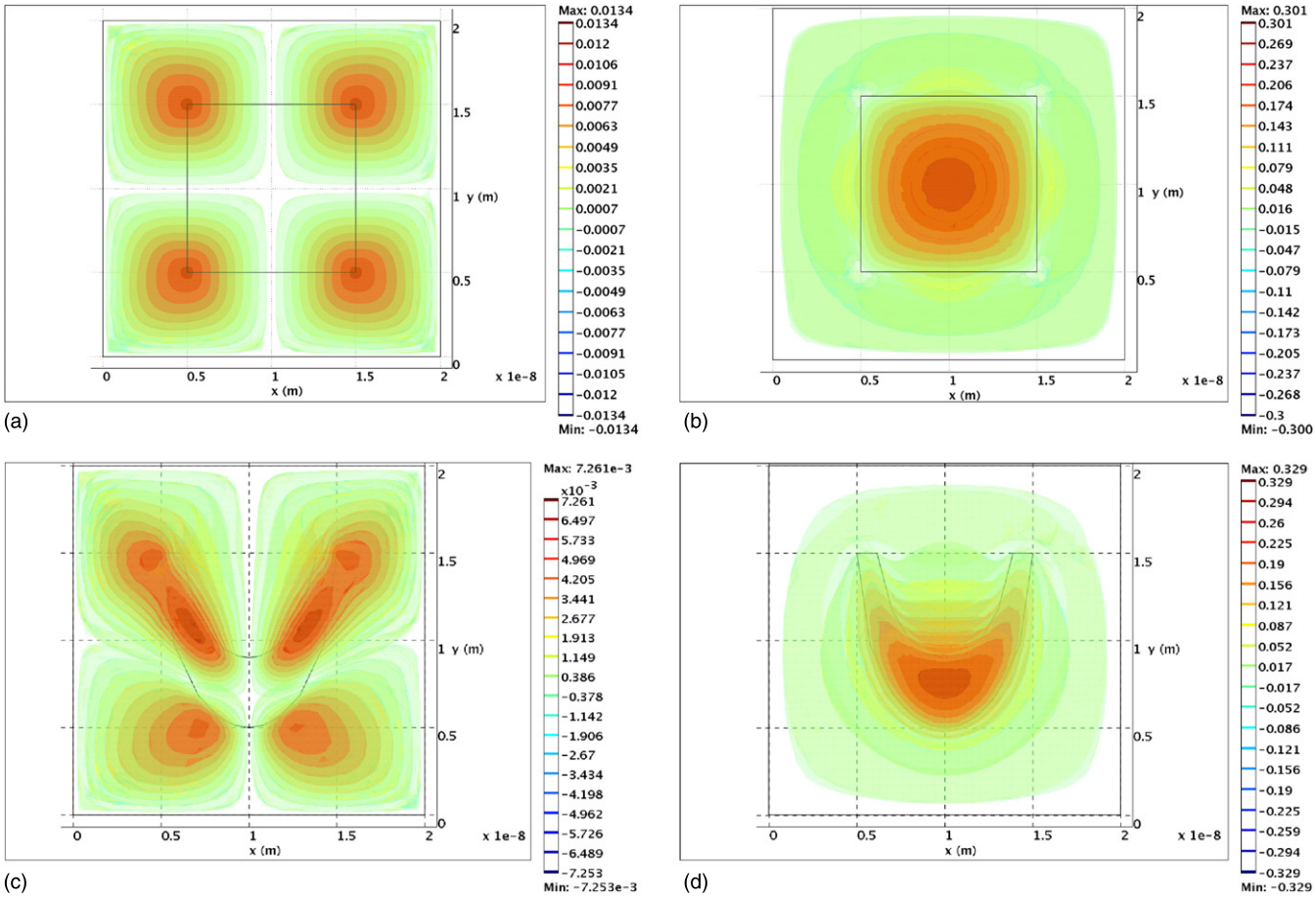

Figure 2. Electric potentials obtained by 3D, numerical calculations, with anisotropy and piezoelectricity. (*a*) V in square shaped CdTe/ZnTe NW. (*b*) V in square shaped CdSe/Cds NW. (*c*) V in crescent shaped CdTe/ZnTe NW. (*d*) V in crescent shaped CdSe/Cds NW. (Colour online.)

(figure 3(*b*)) along the central line and the electric potential (figure 3(*c*)) along the top-right corner line for the triangular, square and crescent CdTe/ZnTe NWs. We plot electric potential at the corners of NWs as they are concentrated along the corners of the NWs (figure 3(*c*)). For the crescent NW, we present an additional plot along the line in the z-direction at $(x, y) = (13.5\,\text{nm}, 11\,\text{nm})$ for the electric potential and electric field as they have the highest magnitudes at that point. The magnitudes of the x-component (y-component) of strain tensor decreases (increases) with an increase in the number of sides required to form the NW geometry. In particular, at the centre of the NW it takes values of $\sim -4.4\%(\sim -4.3\%)$, $\sim -3.2\%(\sim -3.2\%)$ and $\sim -1.4\%(\sim -6.4\%)$ in triangular, square and crescent shaped NWs, respectively. The square NWs have similar values of the x and y-components of the strain tensor as a result of similar contributions from all the directions [17]. As a result of higher values of the initial misfit strain, both the x and y- components of the strain tensor have higher negative values, i.e. the NW is compressively strained in both directions. The z-component of strain tensor, away from the interfaces (inside and outside NWs), in all the NWs is zero. At the interfaces, i.e. at $z = 10$ and 50 nm, the magnitudes of all principal components are much smaller compared with the values at the centre of the NWs. However, near the interfaces it takes a magnitude of $\sim 6\%$, positive outside and negative inside the NWs. The z-components have very high values of the order of $\sim 5.8\%$ for all shaped NWs.

The hydrostatic components inside the NWs are negative as a result of the compressively strained system (figure 3(*b*)). The values are ~ 0.085, ~ -0.061 and ~ -0.078 for triangular, square and crescent-shaped NWs, respectively. At the interfaces it takes positive values ~ 0.021, ~ 0.03 and ~ 0.025, reaching zero while moving sufficiently away from the NW. It should be noted that according to the inclusion based models, the hydrostatic component is constant for the material system and is independent of the geometry and dimensions [17, 27–29], for e.g. in the plane strain case, $\varepsilon_{\text{vol}} = 2\varepsilon_a^*(1-2\nu)/(1-\nu)$). For the CdTe/ZnTe NW system, its value is -0.0366. The differences in its values are about 0.048, 0.025 and 0.041 in triangular, square and crescent, respectively, which is very significant. However, at the interfaces, the differences in the hydrostatic strain components are relatively small, 0.016, 0.006 and 0.011 in triangular, square and crescent NWs, respectively. The hydrostatic strain component is a very important characteristic of the nanostructure systems, as it governs the rigid shift of the energy bands in bandstructures of the respective nanosystems [22]. Therefore proper care should be taken, accounting for this strain component in bandstructure calculations of the strained nanostructures.

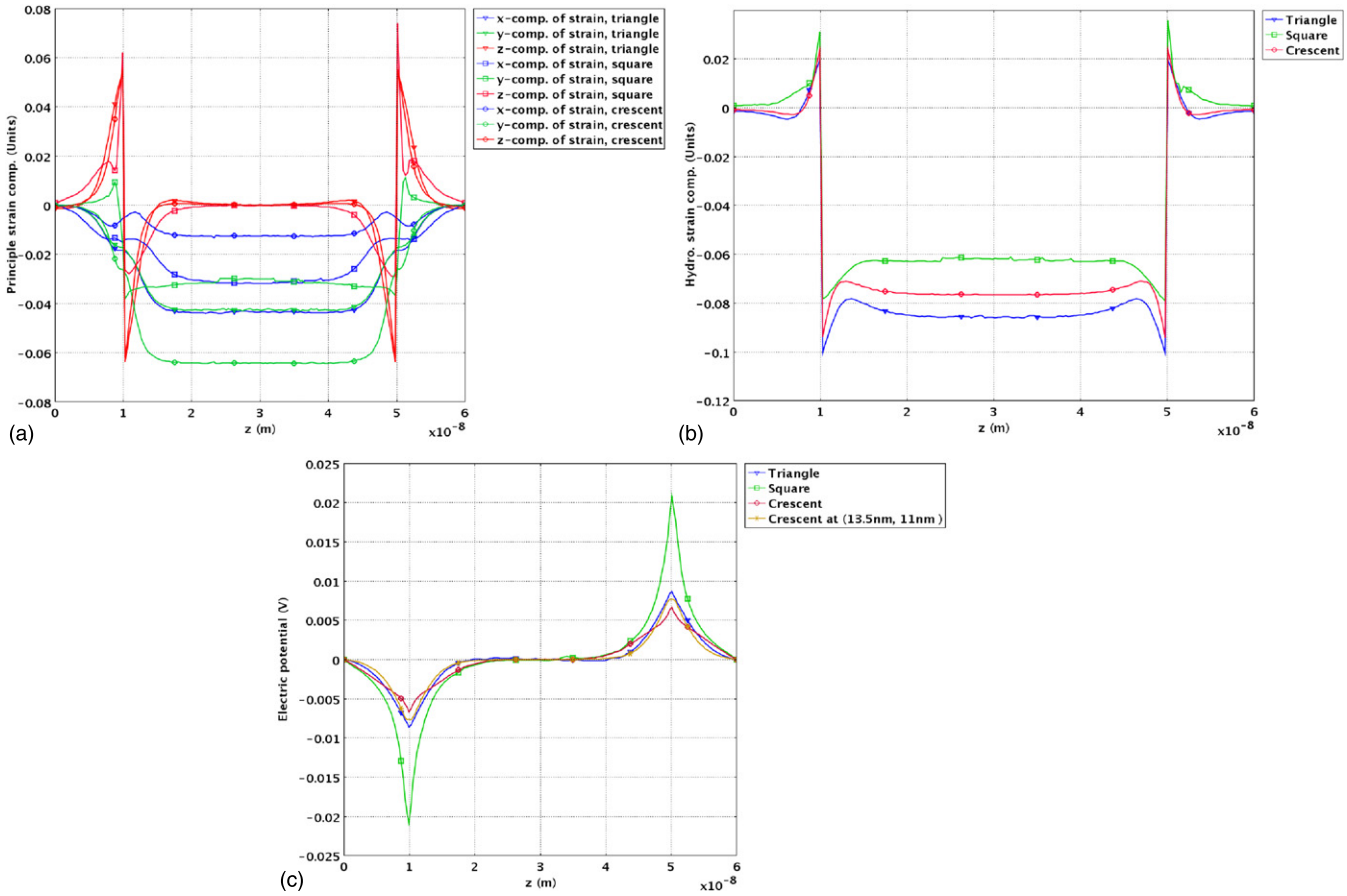

Figure 3. Electromechanical quantities in CdTe/ZnTe NWs along the z-direction. (a) Principle stain components, along the central line in the z-direction. (b) Hydrostatic strain component, ε_{vol}, along the central line in the z-direction. (c) Electric potential, V, along the top-right corner line in the z-direction. (Colour online.)

Strain components have the least magnitudes in square-shaped NWs, i.e. it is the most relaxed CdTe/ZnTe NW geometry among those studied in this contribution. Since piezoelectricity provides an additional degree of freedom for strain accommodation, the electric potential (figure 3(c)) has highest values in the square NW. The maximum and minimum values of electric potential observed in the triangular, square and crescent NWs are $\sim\pm8.0$ mV, $\sim\pm21.0$ mV and $\sim\pm6.5$ mV ($\sim\pm7.5$ mV), respectively. The bracketed value of electric potential is along the line where we observe the highest values of electric quantities, i.e. at $(x, y) = (13.5\,\text{nm}, 11\,\text{nm})$, in the lateral valleys of the crescent-shaped NW. This observation and preference of corners for accumulating electric quantities suggest that the usual practice of neglecting these lateral valleys [17, 28] is not an adequate approximation for studying electromechanical effects in ZB NWs.

Figure 4 shows the principle strain components (figure 4(a)), the hydrostatic strain component, ε_{vol} (figure 4(b)) and the electric potential (figure 4(c)), along the central line, for the triangular, square and crescent CdSe/CdS NWs. Unlike CdTe/ZnTe NWs, the electric potential is concentrated at the centre of the NWs (figures 4(b) and (d)). The magnitudes of the x-component (y-component) of the strain tensor show similar trends to those in CdTe/ZnTe with respect to the geometry of the NWs. However, unlike CdTe/ZnTe NWs, the z-component of the strain tensor is non-zero in all the CdSe/CdS NWs due to an additional mismatch in the z-direction for the WZ crystal. The hydrostatic components inside the NWs are negative and dependent on the geometry of the NW system. The value of hydrostatic strain components is the highest in crescent NW, $\sim-0.074\%$, and the lowest in the square NW, $\sim-0.057\%$, whereas it is $\sim-0.067\%$ in the triangular NW. According to the inclusion based models it is constant for all geometries, 0.033, which again differs substantially from the present results. The strain tensor component has smaller magnitudes in square-shaped NWs, therefore the electric potential has higher magnitudes. The maximum and minimum values of electric potential observed in the triangular, square and crescent NWs are $\sim\pm410$ mV, $\sim\pm520$ mV and $\sim\pm330$ mV, respectively. The values of electromechanical quantities for both material NWs are given in table 2.

In order to study finite length (the z-direction) effects in NWs, we determine electromechanical quantities in CdSe/CdS and CdTe/ZnTe NWs for lengths $L = 40$ nm to $L = 10$ nm, figure 5.

Figure 5(a) shows principal components (x and z) of the strain tensor and hydrostatic strain component, and 5(c) shows the electric potential for square ($L = 40$ nm to 10 nm) CdSe/CdS NWs. It is observed that the magnitude of both principal components of strain tensor increases with

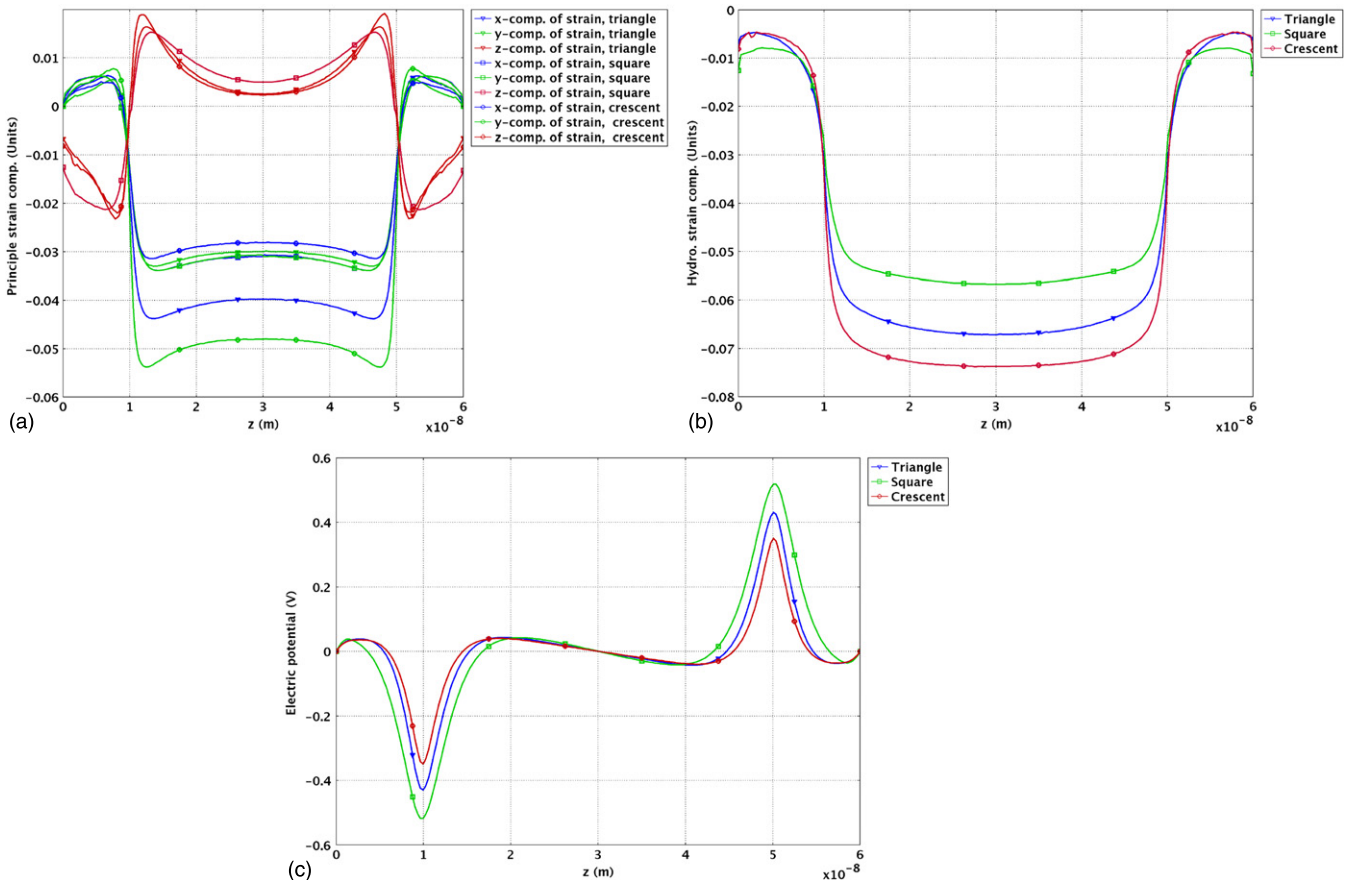

Figure 4. Electromechanical quantities in CdSe/CdS NWs along the z-direction. (a) Principle stain components, along the central line in the z-direction. (b) Hydrostatic strain component, ε_{vol}, along the central line in the z-direction. (c) Electric potential, V, along the central line in the z-direction. (Colour online.)

Table 2. The strain tensor components, potential difference and electric field in the NWs. All values correspond at the central line of the NWs except for *, which correspond to values at the top-right corner of the NW geometries.

NWs	ε_{xx} (%)	ε_{yy} (%)	ε_{vol} (%)	V (mV)
CdTe/ZnTe				
Triangular	−4.4	−4.3	−8.5	16.0*
Square	−3.2	−3.2	−6.1	42.0*
Crescent	−1.4	−6.4	−7.8	13.0*
CdSe/CdS				
Triangular	−4.0	−3.0	−7.4	820
Square	−3.3	−3.2	−5.7	1040
Crescent	−2.8	−4.8	−6.7	660

a decrease in the length of the NW, however hydrostatic component decreases. As there exist different magnitudes of lattice mismatch in the x and z directions, the change in magnitude of the z-component of the strain tensor (from 0.5% at $L = 40$ nm to 3.2% at $L = 10$ nm) is higher compared with the x-component (from 3.1% at $L = 40$ nm to 3.8% at $L = 10$ nm). The hydrostatic strain component also decreases significantly from 5.7% ($L = 40$ nm) to 4.6% ($L = 10$ nm). The electric potential difference across the faces of NWs (figure 5(c)) is almost constant. At $L = 40$ nm it takes value of 0.9 V and slightly decreases to 0.88 V at $L = 20$ nm and then it increases to 0.94 V at $L = 10$ nm. The relatively significant increase in electric potential at $L = 10$ nm is due to a fact that the length of the NW becomes equal to the side of its cross-section and hence contributes equally. Figure 5(b) shows principal components (x and z) of the strain tensor and hydrostatic strain component and figure 5(d) shows the electric potential for square (length, $L = 40$ to 5 nm) CdSe/CdS NWs. Qualitatively and quantitatively, a different length dependence of all electromechanical quantities in CdTe/ZnTe NWs is observed compared with CdSe/CdS NWs. The magnitude of the x-component of the strain tensor decreases with a decrease in length of the NW, ∼3.2% at $L = 40$ nm to ∼1.6% at $L = 10$ nm. The value of the z-component of the strain tensor is ∼0.0 for $L = 40$ nm and 0.3% for 20 nm, while it shows a sharp increase when the length of the NW becomes equal to the side of its cross-section, ∼−2.2% at $L = 10$ nm [22]. As there is no difference in lattice mismatch along the z-direction, the change in the magnitude of the z-component of the strain tensor (∼2.5%) is smaller than the change in the x-component (∼1.8%). The hydrostatic strain component decreases significantly from ∼6.1% (at $L = 40$ nm) to ∼5.3% ($L = 10$ nm). The electric potential difference across the faces of NWs (figure 5(d)) has a decreasing trend with an increase in length, ∼41 mV for $L = 40$ nm, ∼27 mV for $L = 20$ nm and ∼24 mV for $L = 10$ nm. The change in electric potential with a decrease in length is much smaller in CdTe/ZnTe NWs (17.0 mV) as compared with CdSe/CdS NWs (150 mV).

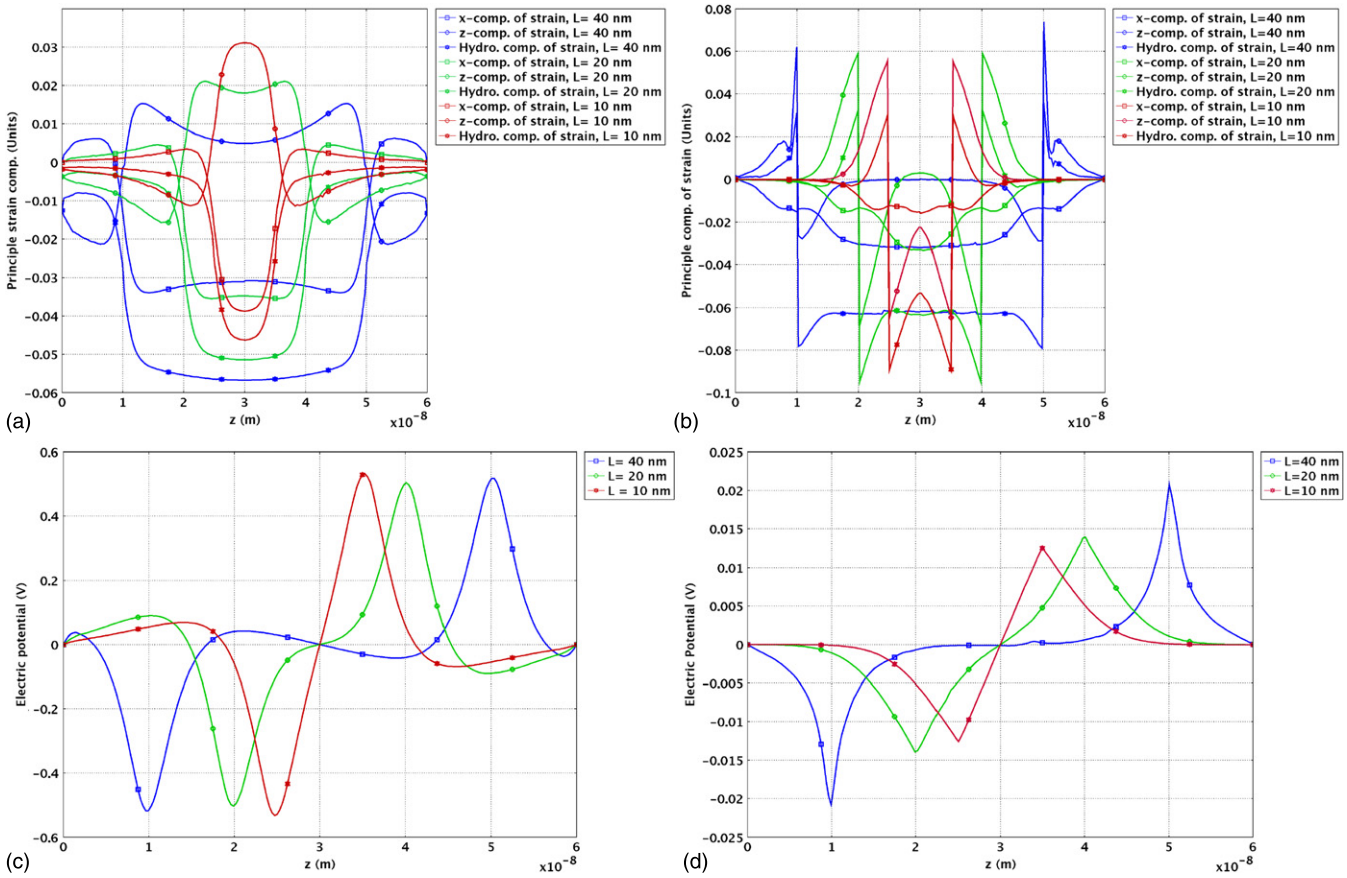

Figure 5. Effect of length on electromechanical quantities in CdSe/CdS and CdTe/ZnTe NWs. (*a*) Principle stain components in CdSe/CdS NWs, along the central line in the z-direction. (*b*) Principle stain components in CdTe/ZnTe NW, along the central line in the z-direction. (*c*) Electric potential, V in CdSe/CdS NWs, along the central line in the z-direction. (*d*) Electric potential, V, in CdTe/ZnTe NWs, along the top-right corner line in the z-direction. (Colour online.)

4. Conclusions

Coupled electromechanical effects in the finite length WZ CdSe/CdS and ZB CdTe/ZnTe NWs of the II–VI group have been studied. The application of our general 3D model demonstrated significant qualitative and quantitative differences in electromechanical distributions in WZ and ZB NWs, compared with the results obtained with frequently used simplified models. The conventional inclusion based methods fail to identify these differences. The hydrostatic strain component is observed to be dependent on the shapes and dimensions of the NWs system while the conventional inclusion based methods predict constant values. Qualitative and quantitative distributions of electromechanical quantities are observed to be significantly different in WZ and ZB NWs. In the case of ZB CdTe/ZnTe, higher values of electric field and potential are observed at corners, whereas in WZ CdSe/CdS they are observed at the interface centres of the NWs. Higher values of electrical quantities in the lateral valleys of crescent-shaped ZB NWs signify that it is not an adequate approximation to neglect such lateral valleys. The finite length of the NWs is another important characteristic that must be accounted for, since the electromechanical parameters vary significantly with the length of the NWs.

Acknowledgments

This work, conducted in the M^{2}NeT Laboratory (http://www.m2netlab.wlu.ca), was made possible by the facilities of the Shared Hierarchical Academic Research Computing Network (SHARCNET). RM acknowledges the support from the NSERC and CRC programme.

References

[1] Yadav R and Pandey K 2006 *Mater. Res. Innov.* **10** 402
[2] Fonoberov V A and Balandin A A 2004 *J. Vac. Sci. Technol.* B **22** 2190
[3] Piprek J 2007 *Nitride Semiconductor Devices: Principles and Simulation* (Weinheim: Wiley)
[4] Andreev A D and O'Reilly E P 2000 *Phys. Rev.* B **62** 15851
[5] Maksimov M V, Krestnikov I L, Ivanov S V, Ledentsov N N and Sorokin S V 1997 *Semiconductors* **31** 800
[6] Hsinchu J 2005 Tri-color ZnSe white light emitting diode US Patent 6919582
[7] Kim T W, Lee E H, Lee K H, Kim J S and Park H L 2003 *Appl. Phys. Lett.* **83** 4235
[8] Woo J T, Song S H, Lee I, Kim T W, Yoo K H, Lee H S and Park H L 2007 *J. Appl. Phys.* **102** 033521
[9] Galan O V, Carbajal A A, Perez R M, Santana G, Hernandez J S, Puente G C, Acevedo A M and Velazquez M T 2006 *Sol. Energy Mater. Sol. Cells* **90** 2221

[10] Liu X, Cai X, Qiao J, Mao J and Jiang N 2003 *Thin Solid Films* **441** 200
[11] Crouse D T, Crouse M, Mahapatra S and Ikram A A 2006 *Nature Nanotechnology* **3** 117
[12] Wen B and Melnik R V N 2008 *Appl. Phys. Lett.* **92** 261911
[13] Onodera C, Shoji T, Hiratate Y and Taguchi T 2007 *Japan. J. Appl. Phys.* **46** 248
[14] Kapon E, Hwang D M and Bhat R 1989 *Phys. Rev. Lett.* **63** 430
[15] Kapon E, Walther M, Christen J, Grundmann M, Caneau C, Hwang D M, Colas E, Bhat R, Song G H and Bimberg D M 1992 *Superlatt. Microstruct.* **12** 491
[16] Maranganti R and Sharma P J 2003 *J. Comput. Theor. Nanosci.* **4** 715
[17] Patil S, Hong W P and Park S H 2008 *Phys. Lett.* A **372** 4076
[18] Melnik R and Mahapatra R 2007 *Comput. Struct.* **85** 698
[19] Patil S, Wen B and Melnik R V N 2008 *29th Int. Conf. on the Physics of Semiconductors (Rio de Janeiro, Brazil) AIP Conf. Proc.* submitted
[20] Patil S, Samani M B, Melnik R V N, Toropova M and Zu J 2008 *29th Int. Conf. on the Physics of Semiconductors (Rio de Janeiro, Brazil) AIP Conf. Proc.* submitted
[21] Sharma N D, Maranganti R and Sharma P 2007 *J. Mech. Phys. Solids* **55** 2328
[22] Downes J R, Faux D A, and O'Reilly E P 1995 *Mater. Sci. Eng.* B **35** 357
[23] Grrundmann M, Stier O and Bimberg D 1994 *Phys. Rev.* B **50** 14187
[24] Williams D P, Andreev A D, O'Reilly E P and Faux D A 2005 *Phys. Rev.* B **72** 235318
[25] Pan E , Albrecht J D and Zhang Y 2007 *Phys. Status Solidi* b **244** 1925
[26] Sun J, Buhro W E, Wang L W and Schrier J 2008 *Nanoletters* **8** 2913
[27] Faux D A, Downes J R, and O'Reilly E P 1996 *J. Appl. Phys.* **80** 2515
[28] Downes J R, Faux D A, and O'Reilly E P 1997 *J. Appl. Phys.* **82** 3754
[29] Downes J R and Faux D A 1995 *J. Appl. Phys.* **77** 2444
[30] Pan E, Han F and Albrecht J D 2005 *J. Appl. Phys.* **98** 013534
[31] Willatzen M, Melnik R V N, Galeriu C and Lew Yan Voon L C 2004 *Math. Comput. Simul.* **65** 385
[32] Lew Yan Voon L C, Lassen B, Melnik R and Willatzen M 2004 *J. Appl. Phys.* **96** 4660
[33] Lassen B, Willatzen M, Melnik R and Lew Yan Voon L C 2004 *J. Mater. Res.* **21** 2927
[34] Radulovic N, Willatzen M, Melnik R V N and Lew Yan Voon L C 2006 *J. Comput. Theor. Nanosci.* **3** 551
[35] Lassen B, Lew Yan Voon L C, Willatzen M and Melnik R 2004 *Solid State Commun.* **132** 141
[36] Faux D A, Howells S G, Bangert U and Harvey A J 1994 *Appl. Phys. Lett.* **64** 1271
[37] Madelung O 2004 *Semiconductors: Data Handbook* 3rd edn (Berlin: Springer)
[38] Nan C W 1994 *Phys. Rev.* B **49** 12619
[39] Bhargava R 1997 *Properties of Wide Bandgap II–VI Semiconductors* (Briarcliff Manor, NY: Institution of Engineering and Technology)
[40] Zaika G A 1994 *J. Math. Sci.* **68** 688
[41] Vij D R 2004 *Handbook of Electroluminescent Materials* (London: Taylor and Francis)
[42] Ukita M, Hiei F, Nakano K and Ishibashi A 1995 *Appl. Phys. Lett.* **66** 209
[43] Maheswarnathan P, Sladek R J and Debska U 1985 *Phys. Rev.* B **31** 7190
[44] Ninomiya S and Adachi S 1995 *J. Appl. Phys.* **78** 1183
[45] Adachi S 2004 *Handbook on Physical Properties of Semiconductors* (Norwell: Kluwer Academic Publishers)
[46] Iwanaga H, Kunishige A and Takeuchi S 2000 *J. Mater. Sci.* **35** 2451
[47] Buschert J R, Pieris F C, Samarth N, Luo H and Furdyna J K 1994 *Phys. Rev.* B **49** 4619
[48] Kanoun M B, Merad A E, Aourag H, Cibert J and Merad G 2003 *Solid State Sci.* **5** 1211
[49] Dutta M, Brown G J, Ramadurai D, Geerpuram D, Yang J, Kohanpour B, Chen C and Stroscio M A 2005 Nonequilibrium carrier dynamics in semiconductors *Proc. of the 14th Int. Conf. (Springer Proc. in Physics)* (*Chicago, USA*)